

Comparison of Sub-Millimeter-Wave Scattering-Parameter Calibrations With Imperfect Electrical Ports

Dylan F. Williams, *Fellow, IEEE*

Abstract—We develop a metric to quantify the accuracy with which measured scattering parameters can be cascaded. We use the metric to compare five rectangular-waveguide calibration and measurement strategies at sub-millimeter wavelengths that correct to differing degrees for electrical-port imperfections.

Index Terms—Calibration, microwave, millimeter-wave, sub-millimeter wave, vector network analyzer.

I. INTRODUCTION

WE DEVELOP a metric that quantifies the impact of unaccounted-for electrical test-port imperfections on the accuracy with which measured scattering parameters of passive circuits can be cascaded. We use the metric to compare the five calibration reference planes listed in Table I in rectangular waveguide at sub-millimeter wavelengths. These calibration reference planes and the corresponding treatment of the interfaces account for test-port imperfections with differing degrees of accuracy, but require different levels of effort to implement.

Most vector network analyzer (VNA) calibrations ignore differences and imperfections in the VNA test ports and the ports of the calibration standards and devices under test. Nevertheless, we have developed some methods in the past that correct for imperfections in the calibration standards and test ports of on-wafer, coaxial and rectangular-waveguide calibrations [1]–[3]. In addition, Hoffmann *et al.* [4] have developed models for coaxial connections and used them to improve calibration accuracy, and some VNA manufacturers have developed proprietary software to accomplish this.

Calibration methods that use dimensional measurements of the test ports and ports of the calibration standards and devices under test to improve calibration accuracy require more effort to implement than traditional calibration approaches. This undoubtedly explains the paucity of work on this class of calibration methods. Nevertheless, as the frequency increases, imperfections in electrical ports become more important. This

makes calibration methods that are able to account for imperfect test ports particularly attractive at sub-millimeter wavelengths, where errors due to mechanical tolerances have much greater impacts on measurement accuracy than at microwave frequencies. This motivates this study of the five calibration strategies and reference planes listed in Table I.

The calibrations and calibration reference planes in Table I are listed in order of difficulty of implementation. The exact calibration method described in [3] places the initial reference plane in the access lines of the device under test, and the scattering parameters of the interfaces between devices must be calculated and included later when devices are cascaded. This calibration is the most accurate, as it rigorously accounts for all of the interfaces during the calibration and measurement process, but requires the greatest effort to perform.

In the split-junction approximation, each junction between calibration standards, devices, and/or test ports is split into two halves, and each half is modeled separately. This approach was used in [4]. Ideally, the calibration reference plane for the measurement is placed in an ideal line attached to the device under test and its two half connectors. Some accuracy is usually sacrificed in this approach, as the scattering parameters of junctions between devices can depend quadratically on the parameters defining the two halves [5]. This approach requires that each interface of the device under test be mechanically characterized, but does not require that the scattering parameters of the interface between devices be calculated later and added between devices when they are cascaded together.

The ideal-reference-plane approximation of [3] places the calibration reference plane for the measurement in an ideal line attached to the test ports of the VNA. This does not require mechanically characterizing the devices under test, but sacrifices some additional accuracy.

The thru-reflect-line (TRL) goal places the reference plane in the access line of the devices under test, but ignores interfaces between devices when cascading. This is equivalent to a perfect TRL calibration. The multiline TRL calibration is the practical implementation of this calibration, and includes the errors due to ignoring the interfaces between calibration standards during the calibration procedure.

II. CALIBRATION APPROACH AND NOMENCLATURE

Our study is based on the general calibration approach introduced in [3], which defines “equivalent” definitions for VNA calibration standards that correct for imperfections in the VNA test ports and the electrical ports of the standards and the device

Manuscript received August 02, 2011; revised August 08, 2011; accepted August 25, 2011. Date of publication October 18, 2011; date of current version January 18, 2012. This work was supported by the Defense Advanced Research Projects Agency’s Terahertz Electronics Program.

The author is with the National Institute of Standards and Technology, Boulder, CO 80305 USA (e-mail: dylan@boulder.nist.gov).

Color versions of one or more of the figures in this paper are available online at <http://ieeexplore.ieee.org>.

Digital Object Identifier 10.1109/TTHZ.2011.2167833

TABLE I
CALIBRATION REFERENCE PLANES ORDERED BY DIFFICULTY OF IMPLEMENTATION

Exact Calibration	Required	Required	In device access line, interfaces added later
Split-Junction Approximation	Required	Required	In ideal line connected to device
Ideal-Reference-Plane Approximation	Required	None	In ideal line connected to VNA test port
TRL Goal	None	None	In device access line, interfaces ignored later
Multiline TRL	None	None	Same, but interface errors in calibration included

under test. Each port of the VNA, calibration standards, and devices under test must be characterized by mechanical measurements, and these mechanical measurements are used to build electrical models for the interfaces between the various ports in the system before the equivalent definitions of [3] can be determined.

For example, the equivalent definition $T_{\text{DEF}}^{\text{LINE}}$ of a transmission-line standard for the exact calibration is defined in [3, eq. (5)] by

$$T_{\text{DEF}}^{\text{LINE}} \equiv [T^{\text{P1/DUT1}}]^{-1} T^{\text{P1/LINE}} T^{\text{LINE}} T^{\text{LINE/P2}} [T^{\text{DUT2/P2}}]^{-1} \quad (1)$$

where T^{LINE} is the cascade matrix of the line, $T^{\text{P1/LINE}}$ is the cascade matrix of the interface between the VNA's test port 1 and port 1 of the line, $T^{\text{LINE/P2}}$ is the cascade matrix of the interface between port 2 of the line and the VNA's test port 2, $T^{\text{P1/DUT1}}$ is the cascade matrix of the interface between the VNA's test port 1 and port 1 of the device under test, and $T^{\text{DUT2/P2}}$ is the cascade matrix of the interface between port 2 of the device under test and the VNA's test port 2. Equivalent definitions for a "flush thru" flat shorts, and other standards are summarized in the Appendix and fully described in [3].

The cascade matrices $T^{\text{P1/DUT1}}$ and $T^{\text{DUT2/P2}}$ of the interfaces between the VNA test ports and the device under test can be defined so as to achieve the different calibration reference planes listed in Table I [3]. When the transmission matrices $T^{\text{P1/DUT1}}$, $T^{\text{P1/LINE}}$, $T^{\text{LINE/P2}}$, and $T^{\text{DUT2/P2}}$ are determined accurately with dimensional measurements and models, the approach rigorously accounts for all of the imperfections in the test, calibration standard, and device ports, and can yield significant improvement in overall calibration accuracy. For example, this method was successfully applied in [5] to 500–750 GHz WM-380 (WR 1.5) rectangular waveguide calibrations, and yielded significant improvements in accuracy.

III. CALIBRATIONS

The calibration strategy of [3] can be tailored to achieve any of the first four calibration reference planes in Table I.

A. Exact Calibration

We refer to the principle calibration discussed in [3] as the exact calibration in Table I because all of the imperfections in the test-port and other electrical interfaces in the calibration, measurement, and cascading process modeled by the dimensional measurements are fully accounted for. Fig. 1(a) illustrates the exact calibration reference plane, and Fig. 1(b) shows how the interfaces between devices under test are added back into the

measurements when cascading devices. Note that this approach always treats interfaces between devices as a whole. This is required if the admittances at the test ports are to be accurately accounted for.

Fig. 2 shows why connections between flanges must be treated as a whole if no approximations are to be made. As discussed in both [3] and [5], the admittances at rectangular-waveguide ports not only become significant at sub-millimeter wavelengths, but are quadratic and depend on the square of the total displacement between ports. Similar behavior is also observed in eccentric coaxial transmission lines. Thus the scattering parameters of the interface between electrical ports cannot be determined by summing contributions to the admittance calculated from the offset of each aperture at each port and its alignment pins separately, but rather must be determined from the total lateral offset between apertures.

As a result of this quadratic dependence of the junction capacitance on the lateral offset, [3] and [5] show that the reference plane of rectangular-waveguide calibrations cannot be placed in the middle of the junction between two guides without introducing significant error. To remedy this, [3] suggests placing the calibration reference planes just inside the interfaces to the device under test, and then mathematically moving the reference plane back to the plane of the interface with a simple reference-plane translation, as shown in Fig. 1(a). Accurately cascading the scattering parameters of devices measured with this procedure requires calculating the scattering parameters of the interface between the two electrical ports of the devices and including them separately in the cascade, as illustrated in Fig. 1(b). While this calibration approach is rigorous, its implementation requires a good deal of "savoir faire."

B. Ideal-Reference-Plane Approximation

Reference [3] suggests an alternative calibration that is easier for the user. In this calibration the final reference plane is placed in an ideal transmission line connected to the VNA test port, and then transformed back to the test port. While this calibration does not properly correct for the interface between the VNA test port and the electrical ports of the devices under test, [3] argues that this is the best that we do without mechanically characterizing the ports of the devices under test. We call this the ideal-reference-plane approximation (see Table I), and [3] provides a prescription for standard definitions that leads to calibrations at this reference plane.

Fig. 1(d) illustrates the reference-plane position for the ideal-reference-plane approximation. While the interfaces between test ports and calibration standards in the ideal-reference-plane approximation are treated rigorously, dimensional measurements of the ports of the devices under test are not used

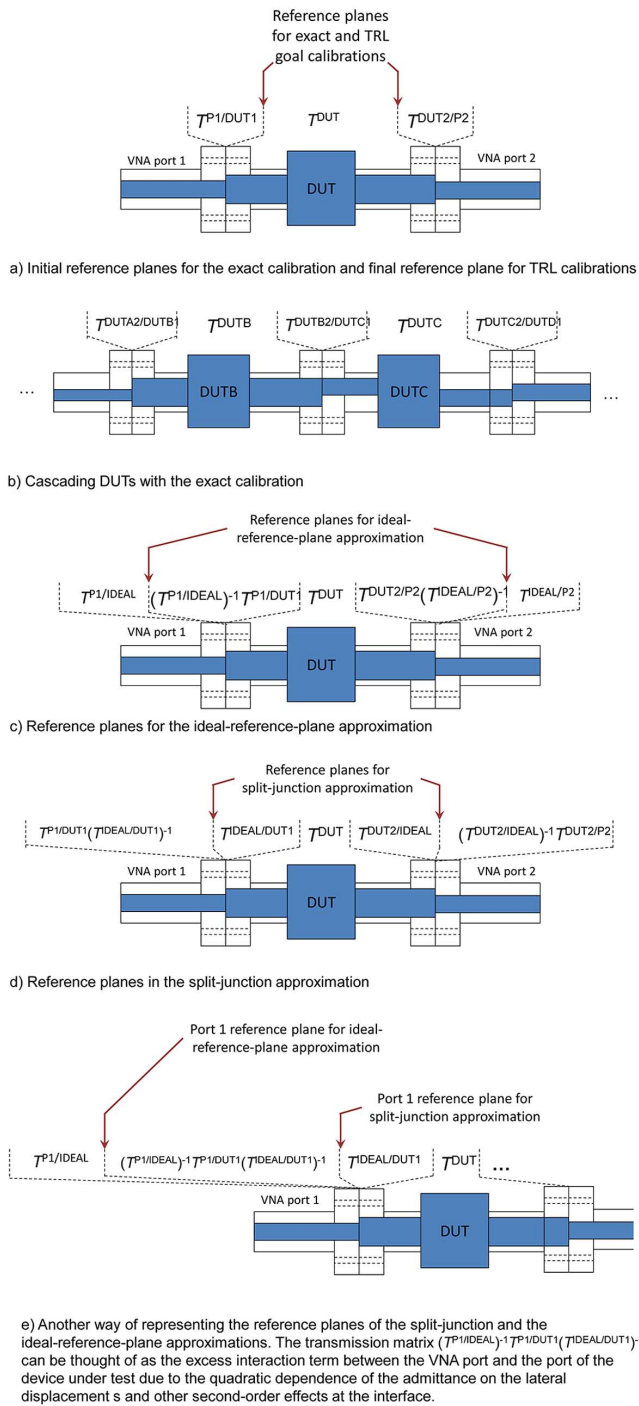


Fig. 1. Calibration reference planes listed in Table I. (a) Initial reference planes for the exact calibration and final reference plane for TRL calibrations. (b) Cascading DUTs with the exact calibration. (c) Reference planes for the ideal-reference-plane approximation. (d) Reference planes in the split-junction approximation. (e) Another way of representing the reference planes of the split-junction and the ideal-reference-plane approximations. The transmission matrix $(\tau^{P1/IDEAL})^{-1} \tau^{P1/DUT1} (\tau^{IDEAL/DUT1})^{-1}$ can be thought of as the excess interaction term between the VNA port and the port of the device under test due to the quadratic dependence of the admittance on the lateral displacement s and other second-order effects at the interface.

to correct properly for the interface between the VNA test ports and the devices under test.

As a consequence, the admittances that depend quadratically on the total displacement between the VNA test port and

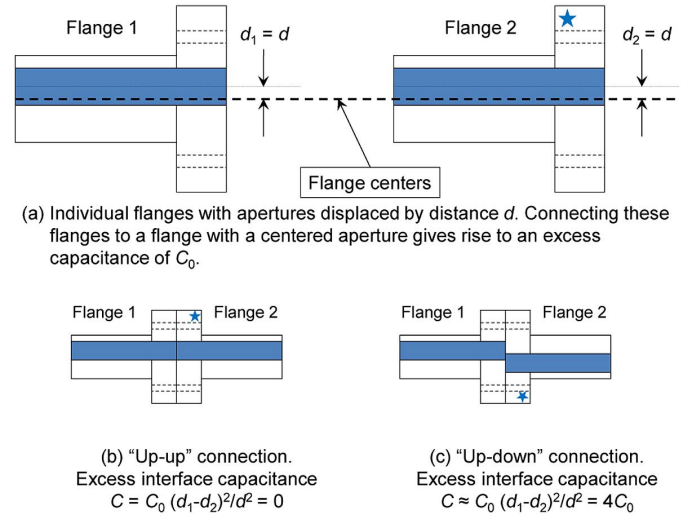


Fig. 2. Quadratic behavior of the admittance at the interface between two flanges makes it impossible to "split" the flanges without some degradation in accuracy. (From [3]). (a) Individual flanges with apertures displaced by distance d . Connecting these flanges to a flange with a centered aperture gives rise to an excess capacitance of C_0 . (b) "Up-up" connection Excess interface capacitance $C = C_0 (d_1 - d_2)^2 / d^2 = 0$. (c) "Up-down" connection Excess interface capacitance $C \approx C_0 (d_1 - d_2)^2 / d^2 = 4C_0$.

the device port in $(\tau^{P1/IDEAL})^{-1} \tau^{P1/DUT1}$ and $\tau^{DUT2/P2} (\tau^{IDEAL/P2})^{-1}$ are lumped into the device under test. While the result is less accurate, dimensional measurements of the electrical ports of the devices are not required, and the user can cascade scattering parameters in the conventional fashion. One of the important goals of this paper is to quantify the degradation in the accuracy of calibrations employing the ideal-reference-plane approximation.

C. Split-Junction Approximation

Other reference planes are also possible. One of those is the split-junction approximation [4] listed in Table I. The split-junction approximation can be viewed as beginning with a measurement of the scattering-parameters of the device under test at the reference plane in Fig. 1(a), and then cascading this result with the scattering parameters of interfaces between the device's initial reference plane and an ideal transmission line calculated from dimensional measurements. The split-junction approximation can also be viewed as a choice of reference-plane position, as shown in Fig. 1(d) and (e).

An important advantage of the split-junction approximation is that unaccounted-for error due to quadratic terms in the ideal-reference-plane approximation do not get "lumped" into the result. However, the split-junction approximation does require dimensional measurements of the devices under test that are not required in the ideal-reference-plane approximation.

While we expect the split-junction approximation to be more accurate than the ideal-reference-plane approximation, the two approximations should converge when the quadratic admittances and other second-order effects at the interface between the VNA test ports and the device ports become small. A second important goal of this paper is to quantify the relative errors of the ideal-reference-plane and split-junction approximations, making it easier to determine when the additional

effort required to arrive at the split-junction approximation is justified.

D. TRL Goal

We will also quantify the improvement possible with these calibrations to the error introduced by leaving out the interfaces between the devices in Fig. 1(b) entirely. That is, we will quantify the error incurred by using the reference plane in Fig. 1(a) without later accounting for the interfaces between the ports of cascaded devices. We call this the TRL goal because the TRL calibration is designed to measure devices at this reference plane.

E. Multiline TRL

Of course, actual TRL calibrations may include error that is not present in the TRL goal reference plane, as TRL calibrations do not use dimensional measurements to account for the imperfections in the interfaces between the VNA test ports and the ports of the calibration standards and devices under test. Thus the error of the TRL goal reference plane is actually a lower bound on the accuracy obtained with actual TRL calibrations.

For this reason, we also investigate multiline TRL calibrations [6]. The calibrations were based on a thru and three lines 3/16th, 1/4, and 5/16th of a wavelength long at the center of the band. These multiline TRL calibrations included errors due to steps in rectangular waveguide heights and widths and lateral aperture misalignments at the interfaces during the calibration procedure.

IV. MEASUREMENT ILLUSTRATION

We performed an experiment in WR-90 rectangular waveguide over the frequency range of 8.2–12.4 GHz that illustrates the advantages and disadvantages of some of the calibration reference planes listed in Table I. During the experiment we used shims to introduce 1.53 and 3.06 mm E-plane offsets between flanges to simulate offsets between the aperture openings and the flange alignment pins of various devices. Similar experiments were discussed in [3].

After characterizing a 1.119 cm long line and a load, we measured the reflection coefficient of the line and load connected in the “up–down” and “up–up” connection configurations shown in Fig. 2 and the insets of Figs. 3 and 4. Both configurations correspond to connecting a line and load with apertures offset from their respective alignment pins by 1.53 mm. However, in the up–down connection configuration, the line and load apertures do not line up, resulting in a total E-plane offset between the apertures of 3.06 mm. In the up–up configuration, on the other hand, the load is flipped upside down before the connection is made, which results in no E-plane offset between the apertures.

The measurements of the actual cascaded line and load are labeled “Direct Measurement” and marked by hollow circles in the figures. The goal of all of the calibrations is to accurately reproduce this direct measurement.

In the up–down connection configuration of Fig. 3, the 3.06 mm offset between the apertures results in a significant admittance at the interface between the line and the load. This leads to

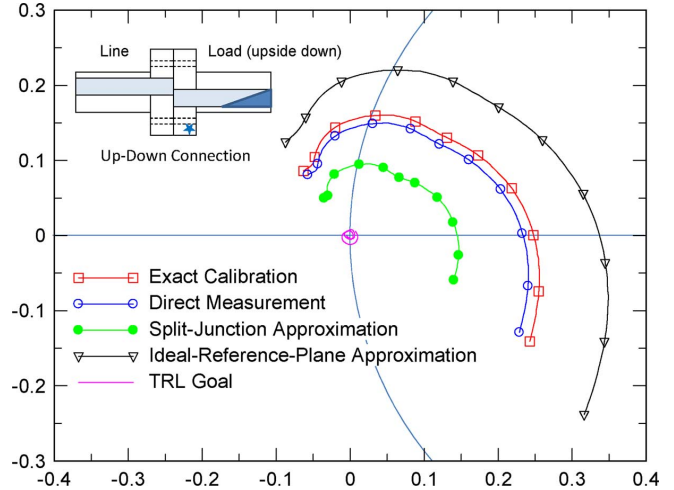


Fig. 3. Estimates of the vector reflection coefficient of a line cascaded with a load in the up–down configuration (shown in the inset) plotted in the interior of the Smith chart. The frequency varies from 8.2 to 12.4 GHz.

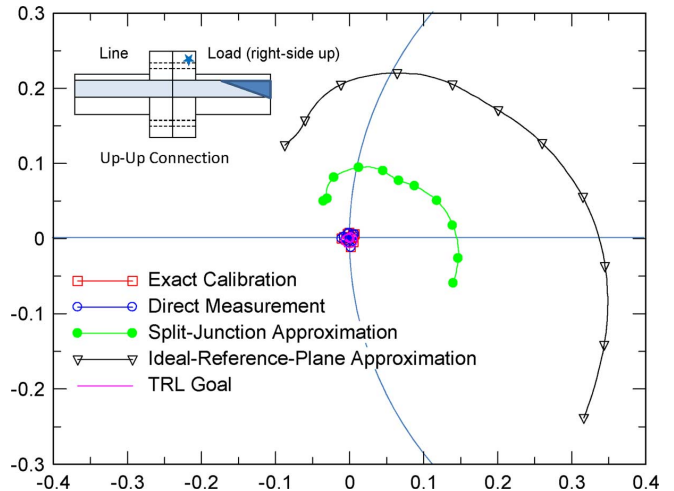


Fig. 4. Estimates of the vector reflection coefficient of a line cascaded with a load in the up–up configuration (shown in the inset) plotted in the interior of the Smith chart. The frequency varies from 8.2 to 12.4 GHz.

reflection coefficients of the cascaded line and load with magnitudes of 0.1–0.2, as shown in the vector plot. However, in the up–up configuration of Fig. 4, the two apertures line up, and the reflection coefficient of the cascaded line and load is nearly an order of magnitude lower.

The other curves in Figs. 3 and 4 show the reflection coefficients of the cascaded line and load predicted from measurements performed at the calibration reference planes of Table I. The TRL goal predicts a low reflection coefficient for the cascade, as it completely ignores the interface between the line and load. This gives the correct answer for the up–up connection configuration of Fig. 4, but fails to account for the large reflection at the interface between the line and load in the up–down connection configuration of Fig. 3.

The exact calibration labeled with hollow squares in the figures yields nearly the correct result in both cases, as expected. On the other hand, the split-junction and ideal-reference-plane

approximations do not predict the correct result in either situation.

Nevertheless, the two figures do illustrate the advantage of the split-junction approximation and a limitation of the ideal-reference-plane approximation: The split-junction approximation yields a reflection coefficient that sits roughly between the measured reflection coefficients obtained with the two connection scenarios. This will usually be the case with the split-junction approximation.

The reflection coefficient obtained from the ideal-reference-plane approximation, on the other hand, does not sit close to either measurement. As we mentioned above, some of the admittance that depends quadratically on the total displacement between the VNA test port and the device port is lumped into the devices under test in the ideal-reference-plane approximation, degrading the result. Thus, we expect, and see clearly in this example, that when these admittances are very large, the errors of the ideal-reference-plane approximation can be large as well, even exceeding the error of the TRL goal.

Even so, it would be premature to dismiss the ideal-reference-plane approximation out of hand. The 1.53 mm E-plane offsets we used in this illustration are much larger than those typically encountered in practice, and we would expect that the ideal-reference-plane and split-junction approximations will converge as the aperture offsets decrease. We will see the impact of this later in the paper when we consider more realistic cases. In addition, the ideal-reference-plane approximation is considerably easier to implement than the split-junction approximation (see Table I), as it does not require that the ports on each device under test be characterized mechanically, a painstaking process.

V. COMPARISON METRIC

We developed a metric for comparing the ability of the calibration reference planes listed in Table I to account for the errors in cascading measurement results. The approach is based on the “calibration-comparison” metric of [7], which determines a bound on the differences of the scattering parameters of passive devices measured by two calibrations. The bound is obtained from a transmission matrix X on port 1 and Y on port 2 mapping one calibrated result into the other.

However, in this context, we bound the difference between the scattering parameters of any passive device and a single interface to a neighboring device determined by the scattering parameters of the device and interface as determined by an approximate calibration (i.e., the split-junction approximation, ideal-reference-plane approximation, TRL goal, or multiline TRL) and the scattering parameters of the device and interface determined by the exact calibration. Thus, we set X on port 1 equal to the cascade of the transmission matrix describing the interface in the approximate calibration and $(T^{\text{DUTA2/DUTB1}})^{-1}$, the inverse of the exact transmission matrix of the interface. We set the transmission matrix Y on port 2 equal to I , where I is the identity matrix, as only one interface appears between each pair of devices cascaded [see Fig. 1(b)]. Following [7], we then define $\delta^X \equiv X - I$ and $\delta^Y \equiv Y - I$. Ignoring δ^Y , whose elements are equal to zero, we substitute δ^X into the formulas (15)–(19) of [7] to obtain the bounds ε_{ij} on $|S'_{ij} - S_{ij}^{\text{exact}}|$, where S'_{ij} are the scattering parameters of the cascade of the interface

determined by the approximate calibration and any passive device, and S_{ij}^{exact} are the scattering parameters of the cascade of the exact interface and the same passive device. Finally, the calibration comparison metric is set equal to the maximum of the four bounds ε_{ij} .

In the case of the TRL goal, the transmission matrix of the interface is the identity matrix, so $X = I(T^{\text{DUTA2/DUTB1}})^{-1}$, and we substitute $\delta^X = (T^{\text{DUTA2/DUTB1}})^{-1} - I$ into of [7, eqs. (15)–(19)], where I is the identity matrix. This determines the worst-case impact of ignoring $T^{\text{DUTA2/DUTB1}}$ of the scattering parameters of the cascade of the interface onto any passive device.

For the ideal-reference-plane approximation, the transmission matrix for the interface is $T^{\text{DUTA2/P2}}(T^{\text{IDEAL/P2}})^{-1}(T^{\text{P1/IDEAL}})^{-1}T^{\text{P1/DUTB1}}$, while the exact transmission matrix is $T^{\text{DUTA2/DUTB1}}$. Here, $T^{\text{DUTA2/P2}}$ is the transmission matrix of the interface of port 2 of the device A to test port 2 of the VNA, $T^{\text{IDEAL/P2}}$ is the transmission matrix of the interface between an ideal transmission line and test port 2 of the VNA, $T^{\text{P1/IDEAL}}$ is the transmission matrix of the interface between test port 1 of the VNA and an ideal transmission line, and $T^{\text{P1/DUTB1}}$ is the transmission matrix of the interface between test port 1 of the VNA and port 1 of device B.

Thus, we calculate the calibration-comparison bound by applying [7, eqs. (15)–(19)] with $\delta^X = T^{\text{DUTA2/P2}}(T^{\text{IDEAL/P2}})^{-1}(T^{\text{P1/IDEAL}})^{-1}T^{\text{P1/DUTB1}}(T^{\text{DUTA2/DUTB1}})^{-1} - I$ and the elements of δ^Y set equal to 0. This choice bounds the error introduced by use of the ideal-reference-plane approximation at one port of the scattering parameters of a passive device.

Finally, for the split-junction approximation, the transmission matrix for the interface is $T^{\text{DUTA2/IDEAL}}T^{\text{IDEAL/DUTB1}}$. Thus the bound on the error is calculated by applying [7, eqs. (15)–(19)] with $\delta^X = T^{\text{DUTA2/IDEAL}}T^{\text{IDEAL/DUTB1}}(T^{\text{DUTA2/DUTB1}})^{-1} - I$ and the elements of δ^Y set equal to 0, and bounds the error introduced in the split-junction approximation when $T^{\text{DUTA2/DUTB1}}$ is approximated by $T^{\text{DUTA2/IDEAL}}T^{\text{IDEAL/DUTB1}}$.

Figs. 5 and 6 estimate how these bounds vary in practice. We performed Monte Carlo simulations to examine the distribution of the bounds in WM-2540 (WR 10) [8] from 75 GHz to 110 GHz for the aperture tolerances of $\pm 25.4 \mu\text{m}$ specified in MIL-DTL-85/3C [9] and the WR-10 lateral-offset tolerances of $97 \mu\text{m}$ specified in [10]. These tolerances are typical of current common practice. The Monte Carlo simulations accounted for steps in waveguide height and width and for lateral waveguide offsets, and employed the models recommended in [5] to calculate the required transmission matrices. While corner rounding, burrs, angular offsets, and other errors were neglected in the Monte Carlo simulations, the study [5] indicates that these error mechanisms are usually of less importance than the height, width, and offset tolerances we considered.

Figs. 5 and 6 show the 10%–90% quantiles of the calibration comparison bound on $|S'_{ij} - S_{ij}^{\text{exact}}|$, where S'_{ij} is the scattering matrix determined by the ideal-reference-plane approximation and S_{ij}^{exact} is the scattering matrix determined by the

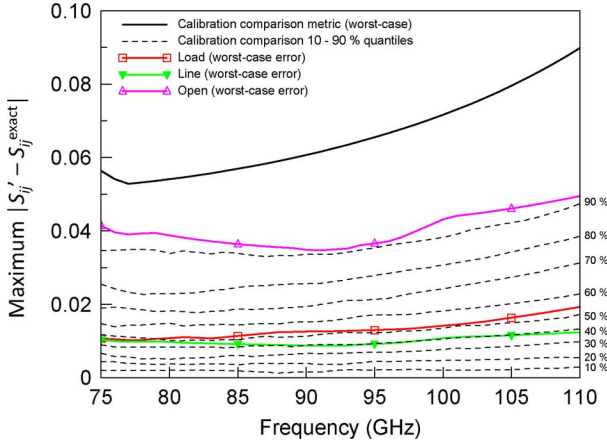


Fig. 5. Calibration-comparison metric is compared to the worst-case deviations of the scattering parameters of three devices from the exact result in WM-2540 (WR 10). We assumed aperture tolerances of $\pm 25.4 \mu\text{m}$ and lateral-offset tolerances of $97 \mu\text{m}$.

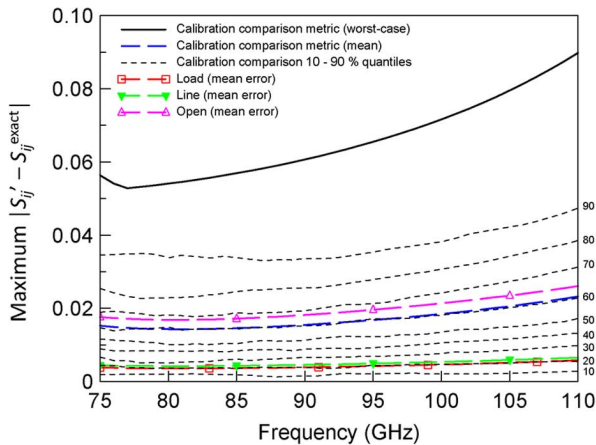


Fig. 6. Calibration-comparison metric is compared to the mean of the difference of the scattering parameters of three devices and the exact result under the same assumptions employed in Fig. 5.

exact calibration. Also plotted on the graphs are the average and worst-case bounds. Finally, the graphs plot the actual mean and worst-case errors introduced by each reference-plane choice in Table I into an open circuit, a load, and a low-loss transmission line with a delay of 0.4 ns .

Fig. 5 shows that the worst-case bound determined from the 200 Monte Carlo simulations only slightly overstates the actual errors observed in the open circuit. Thus we conclude that the worst-case bound does not greatly overestimate the actual worst-case errors that will be encountered in practice, and provides a reasonable metric for assessing the worst-case effect of only partially accounting for the interfaces between devices.

The situation for the mean value of the bound is less clear, as it seems to considerably overstate the average error in the open, load, and transmission line we investigated. Nevertheless, the mean values of the bound obtained from the calibration-comparison metric also seems useful, as they offer another view into the behavior of the deviations.

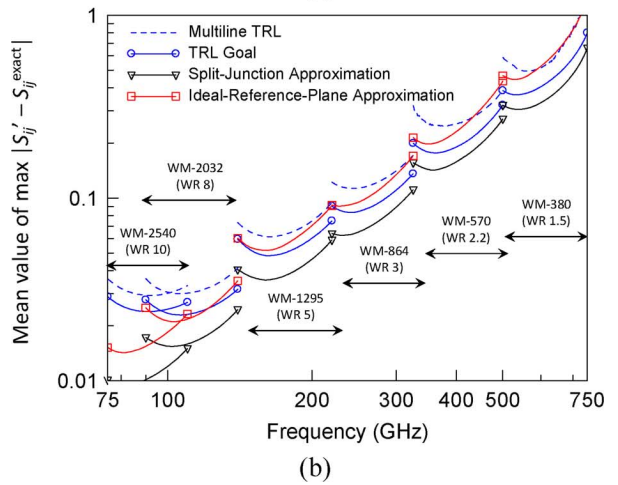
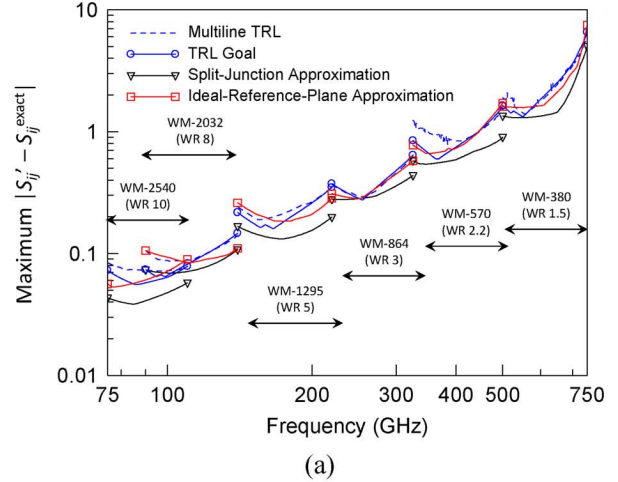


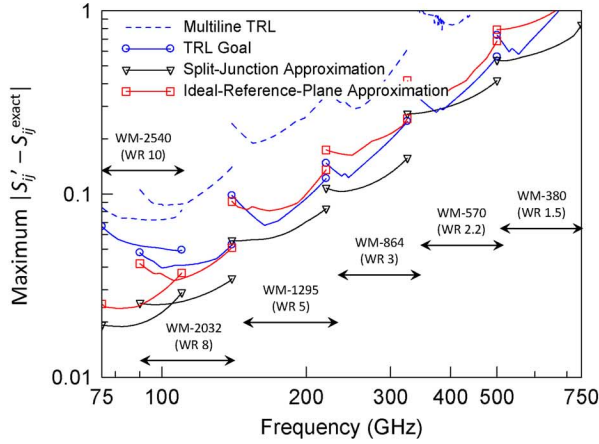
Fig. 7. Worst-case deviations of the scattering-parameters S'_{ij} determined by the calibrations in Table I and the scattering-parameters S_{ij}^{exact} determined by the exact calibration are compared for the WR-10 $97 \mu\text{m}$ tolerance level on lateral flange misalignment. This is the most relaxed of the three lateral tolerance levels we investigate. (a) Worst-case deviations. (b) Mean values of the metric.

VI. COMPARISON OF CALIBRATIONS

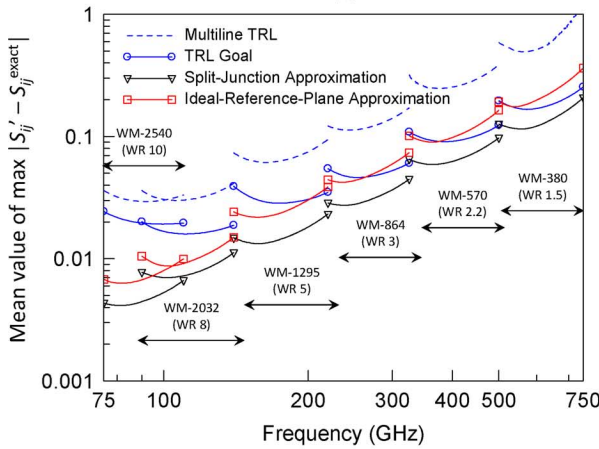
Figs. 7–9 compare worst-case bounds for the split-junction approximation, the ideal-reference-plane approximation, the TRL goal, and multiline TRL calibrations. The figures are all based on the aperture tolerances of $\pm 25.4 \mu\text{m}$ in WM-2540 (WR-10) and $\pm 12.7 \mu\text{m}$ at higher frequencies specified in MIL-DTL-85K [11], but compare the worst-case bounds for different levels of tolerances for lateral flange misalignment.

Fig. 7 compares the bounds for the calibration reference planes listed in Table I at the WR-10 tolerance level for lateral flange misalignment given in [10], which restricts lateral offsets to less than $97 \mu\text{m}$. As we mentioned above, this tolerance level is typical of millimeter-wave flanges in use today.

The figure indicates that, while the split-junction approximation does tend to outperform the ideal-reference-plane approximation and the TRL calibrations, in practice, the differences are probably not of great significance. Only the exact calibration performs significantly better than the other calibrations at these common lateral tolerance levels, and the other logical choice would be easier-to-perform TRL calibration.



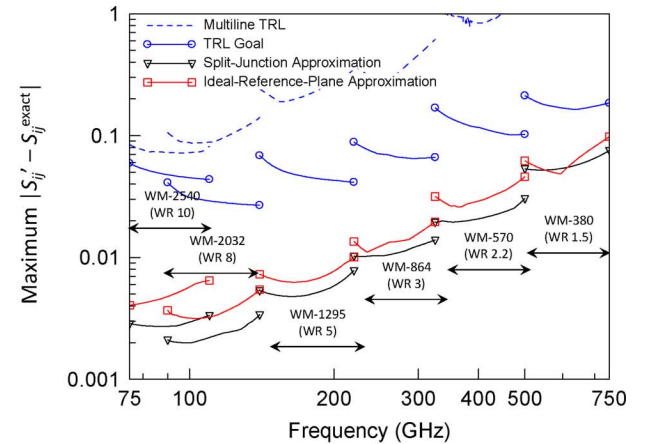
(a)



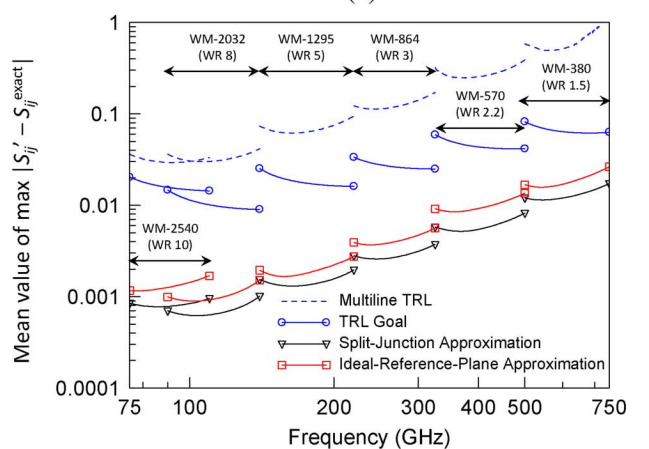
(b)

Fig. 8. Worst-case deviations of the scattering-parameters S'_{ij} determined by the calibrations in Table I and the scattering-parameters S_{ij}^{exact} determined by the exact calibration are compared for the $61 \mu\text{m}$ sub-millimeter tolerance level on lateral flange misalignment. This is representative of the current state of the art in lateral flange misalignment tolerances. (a) Worst-case deviations. (b) Mean values of metric.

The tolerances used to create Fig. 8 correspond to the sub-millimeter tolerances on lateral flange misalignment given in [10], which limit lateral offsets to $61 \mu\text{m}$. This tolerance level is representative of the current state of the art, and is more typical of tolerances currently employed at sub-millimeter wavelengths. Here the split-junction approximation, the ideal-reference-plane approximation and the TRL goal, which correct for interfaces in the calibration process itself using the procedures outlined in [3], are significantly better than results we would expect to obtain from actual multiline TRL calibrations. Nevertheless, the differences between the split-junction approximation, the ideal-reference-plane approximation and the TRL goal are small except in WM-2540 (WR-10), where the split-junction and ideal-reference-plane approximations begin to significantly outperform the TRL goal. However, at all of the higher-frequency bands, only the exact calibration offers significant improvements in accuracy over the split-junction approximation, the ideal-reference-plane approximation and the TRL goal, albeit at the expense of considerable effort in implementation.



(a)



(b)

Fig. 9. Worst-case deviations of the scattering-parameters S'_{ij} determined by the calibrations in Table I and the scattering-parameters S_{ij}^{exact} determined by the exact calibration are compared using the goal for new ultra-precise $14 \mu\text{m}$ tolerance levels proposed by the IEEE P1785 Working Group for lateral flange misalignment. This is well below the tolerances in current use. (a) Worst-case deviations. (b) Mean values of the metric.

Fig. 9 compares the bounds for the calibration reference planes listed in Table I at the $14 \mu\text{m}$ tolerance level on flange misalignment recently proposed as a goal by the IEEE P1785 Working Group [8]. This figure shows that, when lateral tolerances are kept very tight, reducing interface admittances to a minimum, both the split-junction and the ideal-reference-plane approximations significantly outperform the TRL calibrations. This is particularly true at lower frequencies where differences in aperture size become even more important than lateral offsets.

This argues for use of either the split-junction or ideal-reference-plane approximations in place of the more accurate, but more difficult to implement, exact calibration approach only at these lower frequencies, where tolerances on aperture size dominate interface admittances. While the split-junction approximation consistently outperforms the ideal-reference-plane approximation in this low-tolerance limit, the improvement in this range over the easier-to-implement ideal-reference-plane approximation is only modest.

VII. CONCLUSION

Our comparison shows that only the exact calibration of [3], with its inherent difficulty of implementation, can significantly improve the accuracy of sub-millimeter rectangular-waveguide calibrations at the tolerance levels in current use. At these common tolerance levels, we can choose between (a) the most accurate, but also most difficult to implement, exact calibration and (b) the easy-to-implement TRL calibration.

However, this situation changes at the very tight tolerance levels being proposed by the IEEE P1785 Working Group, and more so at lower frequencies than at higher frequencies. At the extremely tight lateral tolerances on waveguide-flange misalignment being proposed by the IEEE P1785 Working Group, our comparison indicated that both the split-junction and ideal-reference-plane approximations begin to significantly outperform TRL calibrations. While neither of these calibrations can outperform the exact calibration, they do eliminate most of the error due to imperfect ports in this limit and are significantly easier to implement than the exact calibration. Here, the ideal-reference-plane approximation, which requires no mechanical measurements of the devices under test, becomes particularly attractive, as it offers accuracy similar to the split-junction approximation without requiring mechanical characterization of each device being tested.

Returning to Table I, we now see that, as a rule of thumb, more effort is required to implement the calibration reference planes with greater accuracy. That said, applying the calibration comparison metric we developed here is offers a good guide to choosing a calibration approach and reference plane, as the degree of improvement depends very much on the frequency and the levels of error due to aperture size and lateral displacement.

APPENDIX

EQUIVALENT CALIBRATION-STANDARD DEFINITIONS

The equivalent definition $T_{\text{DEF}}^{\text{LINE}}$ given in (1) was derived in [3] from the requirement that any device measured by the calibration transforms correctly to the calibration reference plane. Similar arguments can be applied to a flush-thru connection. Reference [3] shows that the equivalent definition $T_{\text{DEF}}^{\text{THRU}}$ of a flush-thru connection is

$$T_{\text{DEF}}^{\text{THRU}} \equiv [T^{\text{P1/DUT1}}]^{-1} T^{\text{P1/P2}} [T^{\text{DUT2/P2}}]^{-1}, \quad (2)$$

where $T^{\text{P1/P2}}$ is the cascade matrix of the interface between the two VNA test ports. Note that this equivalent definition contains fewer cascade matrices than (1). This is expected, as the flush-thru connection is formed by connecting the two VNA ports together and has only a single interface.

The equivalent definition $T_{\text{DEF}}^{\text{SHORT}}$ of a flat short is defined in (9) of [3] by

$$T_{\text{DEF}}^{\text{SHORT}} \equiv [T^{\text{P1/DUT1}}]^{-1} T^{\text{SHORT}} [T^{\text{DUT2/P2}}]^{-1}, \quad (3)$$

where T^{SHORT} are the transmission parameters of the short-circuited test ports. As discussed in [3], most discontinuities in rectangular waveguide can be described as shunt admittances or impedance transformations. As a short has an impedance equal

to 0, applying an impedance transformation to a short or adding a shunt admittance in parallel with a short does not change the impedance of the combination, which remains zero. Thus, in rectangular waveguide, T^{SHORT} corresponds closely to the scattering parameters of a perfect short. Of course, this is a special case, and would not happen if, for example, the test port had discontinuities that could be modeled as a series resistance or inductance.

The equivalent definition $T_{\text{DEF}}^{\text{OFFSET}}$ of an offset standard is defined in [3, eqs. (10) and (11)] by

$$T_{\text{DEF}}^{\text{OFFSET}} \equiv [T^{\text{P1/DUT1}}]^{-1} T^{\text{P1/OFF}} T^{\text{OFF}} T^{\text{STD}} T^{\text{OFF}} \times T^{\text{OFF/P2}} [T^{\text{DUT2/P2}}]^{-1} \quad (4)$$

where $T^{\text{P1/OFF}}$ is the cascade matrix of the interface between test port 1 of the VNA and the transmission-line offset, T^{OFF} is the cascade matrix of the transmission-line offset, and T^{STD} is the cascade matrix of the offset standard.

As mentioned in the text and discussed in [3], the transmission matrices $T^{\text{P1/DUT1}}$ and $T^{\text{DUT2/P2}}$ set the reference plane of the calibration. The exact calibration and TRL goal use the equivalent definitions in (1)–(4). In order to conform with conventional practice, the reference plane would usually be translated back to the interface. The difference between the exact calibration and the TRL goal is that, to achieve the exact result, the transmission matrices corresponding to the interfaces between devices must be included when devices are later cascaded.

Referring to Fig. 1, we see that the ideal-reference-plane approximation is achieved by replacing $T^{\text{P1/DUT1}}$ in (1)–(4) with $T^{\text{P1/IDEAL}}$, the cascade matrix of the transition between port 1 of the VNA and an ideal line, and by replacing $T^{\text{DUT2/P2}}$ with $T^{\text{IDEAL/P2}}$.

Again referring to Fig. 1, the split-junction approximation is achieved by replacing $T^{\text{P1/DUT1}}$ in (1)–(4) with $T^{\text{P1/DUT1}} (T^{\text{IDEAL/DUT1}})^{-1}$ and $T^{\text{DUT2/P2}}$ with $(T^{\text{DUT2/IDEAL}})^{-1} T^{\text{DUT2/P2}}$.

ACKNOWLEDGMENT

The views, opinions, and/or findings contained in this article/presentation are those of the author/presenter and should not be interpreted as representing the official views or policies, either expressed or implied, of the Defense Advanced Research Projects Agency or the U.S. Department of Defense.

REFERENCES

- [1] A. Lewandowski, D. F. Williams, P. D. Hale, C. M. Wang, and A. Dienstfrey, "Covariance-based VNA uncertainty analysis for time- and frequency-domain measurements," *IEEE Trans. Microw. Theory Techn.*, vol. 58, no. 7, pp. 1877–1886, July 2010.
- [2] D. F. Williams and D. K. Walker, "Compensation for geometrical variation in coplanar waveguide probe-tip calibration," *IEEE Microw. Wireless Compon. Lett.*, vol. 7, no. 4, pp. 97–99, Apr. 1997.
- [3] D. F. Williams, "Rectangular-waveguide vector-network-analyzer calibrations with imperfect test ports," in *Autom. RF Techn. Group Conf. Dig.*, Dec. 2010, vol. 76, pp. 1–8.
- [4] J. P. Hoffmann, P. Leuthman, J. Ruefenacht, and K. Wong, "S-parameters of slotted and slotless coaxial connectors," in *Autom. RF Techn. Group Conf. Dig.*, Dec. 2009, vol. 74, pp. 1–5.
- [5] D. F. Williams, "500 GHz–750 GHz rectangular-waveguide vector-network-analyzer calibrations," *IEEE Trans. Terahertz Sci. Technol.*, vol. 1, no. 2, Nov. 2010.

- [6] R. B. Marks, "A multi-line method of network analyzer calibration," *IEEE Trans. Microw. Theory Techn.*, vol. 39, no. 7, pp. 1205–1215, Jul. 1991.
- [7] D. F. Williams, R. B. Marks, and A. Davidson, "Comparison of on-wafer calibrations," in *Autom. RF Techn. Group Conf. Dig.*, Dec. 1991, vol. 38, pp. 68–81.
- [8] N. M. Ridler, R. A. Ginley, J. L. Hesler, A. R. Kerr, R. D. Pollard, and D. F. Williams, "Towards standardized waveguide sizes and interfaces for submillimeter wavelengths," in *21st Int. Symp. Space Terahertz Technol.*, Mar. 2010.
- [9] *Detail Specification Sheet: Waveguides, Rigid, Rectangular (Millimeter Wavelength)*, MIL-DTL-85/3C ed, U.S. Department of Defense, 2005.
- [10] J. L. Hesler, A. R. Kerr, W. Grammer, and E. Wollack, in *18th Int. Symp. Space Terahertz Technol.*, Mar. 2007.
- [11] *Detail Specification: Waveguides, Rigid, Rectangular*, MIL-DTL-85K ed, U.S. Department of Defense, 2011.



Dylan F. Williams (M'80–SM'90–F'02) received the Ph.D. degree in electrical engineering from the University of California, Berkeley, in 1986.

He joined the Electromagnetic Fields Division of the National Institute of Standards and Technology, Boulder, CO, in 1989, where he develops metrology for the characterization of monolithic microwave integrated circuits and electronic interconnects. He has published over 80 technical papers.

Dr. Williams is the recipient of the Department of Commerce Bronze and Silver Medals, two Electrical Engineering Laboratory's Outstanding Paper Awards, two Automatic RF Techniques Group (ARFTG) Best Paper Awards, the ARFTG Automated Measurements Technology Award, and the IEEE Morris E. Leeds Award. He also served a four-year term as Editor-in-Chief of the IEEE TRANSACTIONS ON MICROWAVE THEORY AND TECHNIQUES.